

Heavy quasiparticles in the ferromagnetic superconductor  $\text{ZrZn}_2$ 

S. J. C. Yates, G. Santi, S. M. Hayden, P. J. Meeson, and S. B. Dugdale  
 H. H. Wills Physics Laboratory, University of Bristol,  
 Tyndall Avenue, Bristol BS8 1TL, United Kingdom  
 (Dated: April 14, 2024)

We report a study of the de Haas-van Alphen effect in the normal state of the ferromagnetic superconductor  $\text{ZrZn}_2$ . Our results are generally consistent with an LMTO band structure calculation which predicts four exchange-split Fermi surface sheets. Quasiparticle effective masses are enhanced by a factor of about 4.9 implying a strong coupling to magnetic excitations or phonons. Our measurements provide insight into the mechanism for superconductivity and unusual thermodynamic properties of  $\text{ZrZn}_2$ .

The recent reports of the coexistence of ferromagnetism and superconductivity in  $\text{UGe}_2$  [1],  $\text{ZrZn}_2$  [2],  $\text{URhGe}$  [3] as well as the discovery of superconductivity in the non-magnetic hcp phase of Fe under pressure [4] have reopened the debate regarding the relationship of magnetism and superconductivity. Motivated by the case of liquid  $^3\text{He}$ , the search for superconductivity mediated by spin fluctuations in nearly magnetic materials has a long history [5]. The observation of superconductivity in the ferromagnetic phase of  $\text{ZrZn}_2$  [2] (as well as  $\text{UGe}_2$  and  $\text{URhGe}$ ) together with the extreme sensitivity of its occurrence to sample purity [2, 6], make it a strong candidate for magnetically mediated and spin-triplet superconductivity, as is believed to exist in  $\text{Sr}_2\text{RuO}_4$  [6, 7], although other scenarios are not excluded [8].

A detailed knowledge of the electronic structure of  $\text{ZrZn}_2$  is crucial to the understanding of both its normal and superconducting properties. Thus we report here a detailed study of the Fermi surface (FS) made using angle-resolved measurements of the de Haas-van Alphen effect (dHvA). Our results are compared with an ab-initio electronic structure calculation. We observe much of calculated Fermi surface which consists of four exchange-split sheets. Our study shows that  $\text{ZrZn}_2$  is characterized by a large quasiparticle density-of-states (DOS) at the Fermi energy in the ferromagnetic state, which arises partly from the band structure and partly from a large mass enhancement.

$\text{ZrZn}_2$  has many unusual properties. Below  $T_{\text{FM}} = 28.5 \text{ K}$  it becomes ferromagnetic with an ordered moment of  $0.17 \mu_B$  per formula unit at low temperatures ( $T = 2 \text{ K}$ ). The intrinsic moment is unsaturated, with an applied magnetic field of 6 Tesla causing a 50% increase. Compared with other d-band metals, it has an extremely large electronic heat capacity at low temperatures  $C = T = 47 \text{ mJ K}^{-2} \text{ mol}^{-1}$ .  $\text{ZrZn}_2$  crystallizes in the C15 cubic Laves structure, with lattice constant  $a = 7.393 \text{ \AA}$ , the Zr atoms forming a tetrahedrally co-ordinated diamond structure. Its magnetic properties derive from the Zr 4d orbitals, which have a significant direct overlap.

Interest in  $\text{ZrZn}_2$  has been rekindled by the discovery that it is superconducting at ambient pressure and that both the superconductivity and ferromagnetism are si-

multaneously destroyed by the application of hydrostatic pressure. For the samples considered here, the onset temperature for the superconductivity is  $T_{\text{SC}} = 0.6 \text{ K}$  with  $B_{\text{c2}} = 0.9 \text{ T}$ . The most striking feature of  $\text{ZrZn}_2$ ,  $\text{UGe}_2$  and  $\text{URhGe}$  is perhaps that the same electrons are thought to participate both to superconductivity and ferromagnetism, in contrast with the situation in other "magnetic" superconductors e.g. borocarbides,  $\text{RuSr}_2\text{GdCu}_2\text{O}_8$  [9], where the magnetism and superconductivity occur in different parts of the unit cell. Furthermore,  $\text{ZrZn}_2$  is a three-dimensional intermetallic compound in which the itineracy of the d-electrons is almost unquestionable, whereas some doubts remain about that of the 5f electrons and roles of the strong magnetocrystalline anisotropy and quasi-two-dimensional electronic structure in  $\text{UGe}_2$  and  $\text{URhGe}$ .

The dHvA effect is due to the quantization of the cyclotron motion of charge carriers and results in a magnetization,  $M_{\text{osc}}$ , which oscillates with magnetic field,  $B$ . We interpret our results using the Lifshitz-Kosevich expression [10] in which each extremal area  $A$  of a FS sheet perpendicular to  $\hat{B}$  gives a contribution to the oscillatory magnetization,

$$M_{\text{osc}} / B^{\frac{1}{2}} R_D R_T \sin \frac{2\pi F}{B} + \dots; \quad (1)$$

where  $F(\hat{B}) = (\hbar/2e)A(\hat{B})$ .  $R_D$  and  $R_T$  are the Dingle and temperature damping factors, respectively. The temperature dependence of  $M_{\text{osc}}$  yields the cyclotron mass,  $m$ , through  $R_T = X / \sinh X$  where  $X = 2\pi^2 k_B T / \hbar \omega_c$  and  $\omega_c = eB/m$ . This mass includes all many-body renormalizations and is related to the corresponding orbit through,

$$m = \frac{\hbar}{2} \frac{1}{\text{FS orbit}} \frac{dA}{dF}; \quad (2)$$

The quasiparticle lifetime,  $\tau$ , and the mean-free-path,  $l$ , can be determined on each orbit via the field-dependent factor  $R_D = \exp(-\pi l / v_F \tau)$ . Eq. (1) shows no "spin-splitting factor" [10] since in a ferromagnet, spin-split sheets of the FS are resolved separately.

The dHvA magnetization was measured using a standard low-frequency field-modulation technique. Data

were collected using a top-loading dilution refrigerator equipped with a 13.5 T magnet reaching temperatures as low as 30 mK and with a  $^3\text{He}$  system equipped with an 18 T magnet. High-quality samples ( $\rho_0 = 0.6 \text{ cm}$ ) were prepared by directional cooling of a  $\text{ZrZn}_2$  melt contained in an  $\text{Y}_2\text{O}_3$  crucible inside a tantalum bomb [11].

We performed angle-resolved dHvA measurements for fields applied perpendicular to the [001] and [110] directions. Fig. 1(a) shows a typical Fourier transform of our dHvA data collected for  $\hat{B}$  close to [111]. The spectrum is dominated by the low frequencies  $F = 1.42 \text{ kT}$  and  $F = 1.60 \text{ kT}$  and their harmonics. These frequencies have been previously assigned to an exchange-split pocket of the Fermi surface centered on the  $\Gamma$  point of the Brillouin zone [see Fig. 2(a)]. The frequency difference  $F_{\#} - F_{\#}$  is a measure of the ferromagnetic exchange splitting in  $\text{ZrZn}_2$ . In addition to  $\Gamma_{30}$  and  $\Gamma_{30}$ , we also observe a number of closely spaced frequencies in the range 1.6 { 2.5 kT ( $\Gamma_{27;\#}$ ,  $\Gamma_{27;\#}$ ,  $\Gamma_{27;\#}$ ,  $\Gamma_{27;\#}$ , and  $\Gamma_{27;\#}$ ) and a strong component ( $F_{\#}$ ) near 3.2 kT. Some frequency branches ( $\Gamma_{27;\#}$  and  $\Gamma_{27;\#}$ ) appear as multiplets. In all, our study revealed 17 frequency branches, whose angular dependence is shown in Fig. 1(b). Our results are in good agreement with previous dHvA studies of  $\text{ZrZn}_2$  in which the  $\Gamma_{30}$  and  $\Gamma_{30}$  branches were observed [12]. In addition to extremal FS areas, the temperature dependence of the dHvA amplitude enables the determination of the cyclotron effective mass corresponding to each orbit (see Table I) from the factor  $R_T$  in Eq. (1).

In order to understand our results we performed self-consistent spin-polarized band structure calculations using the LMTO method within the local-spin-density approximation (LSDA) [13]. We obtained a relaxed lattice constant,  $a = 7.223 \text{ \AA}$  and a magnetic moment,  $\mu = 0.18 \mu_B/\text{Zr}$  in excellent agreement with the measured one (of  $0.17 \mu_B/\text{Zr}$  [2]). Our calculation agrees well with others in the literature [8, 14]. The resulting FS and DOS are shown in Fig. 2. The angular dependence of the dHvA frequencies [see Fig. 1(c)] in poses strong constraints on the possible topologies of the FS and is therefore an important tool in verifying the validity of the calculated FS. The cyclotron band mass for each extremal orbit (see Table I) is obtained from the relation  $m_b = (\hbar^2/2) (\partial A/\partial E)_{E_F}$  by numerical differentiation with a  $E_F$  of 0.5 mRy.

The ab-initio calculated FS appears to reproduce the essential topology of the observed one. We assign  $\Gamma_{30}$  and  $\Gamma_{30}$  to the spin-split spherical FS sheet  $\Gamma_{30}$  as in previous studies [12]. The complex of branches observed near [111] including  $\Gamma_{27;\#}$ ,  $\Gamma_{27;\#}$ ,  $\Gamma_{27;\#}$ , and  $\Gamma_{27;\#}$  appears to be due to orbits associated with the X-centered "pillow" features of band 27. Both spin  $\uparrow$  and  $\downarrow$  FS sheets show this feature, thus there are pairs of exchange-split branches such as  $\Gamma_{27;\#}$  and  $\Gamma_{27;\#}$  and  $\Gamma_{27;\#}$  and  $\Gamma_{27;\#}$ . The  $\Gamma_{27;\#}$  branch is probably obscured by the strong  $\Gamma_{30}$  branch near the [110] direction, only allowing detection near [111]. Another prominent

TABLE I: Experimental and calculated dHvA frequencies and cyclotron masses for the principal high-symmetry directions in  $\text{ZrZn}_2$  for  $\hat{B} \parallel [111]$ . Branch assignments refer to Fig. 1(b) and the FS orbits are denoted by orbit center, band index and spin ( $\uparrow$  is the majority).

| Experiment |        |           | Calculation               |        |           |
|------------|--------|-----------|---------------------------|--------|-----------|
| branch     | F (kT) | $m_b/m_e$ | FS Orbit                  | F (kT) | $m_b/m_e$ |
| [110]      |        |           |                           |        |           |
|            | 1.425  | 0.81(4)   | $\Gamma_{30;\#}$ (sphere) | 1.193  | 0.24      |
|            | 1.600  | 0.95(5)   | $\Gamma_{30;\#}$ (sphere) | 1.329  | 0.26      |
|            | 1.810  | 1.27(3)   | $X_{27;\#}$ (pillow)      | 1.438  | -0.51     |
|            | 3.400  | 3.7(10)   | $X_{28;\#}$ (dog bone)    | 4.227  | -2.19     |
|            | 4.770  | 3.9(2)    | $X_{28;\#}$ (dog bone)    | 5.538  | -1.53     |
|            | 5.300  | 3.5(10)   |                           |        |           |
|            |        |           | $X_{29;\#}$ (dog bone)    | 5.541  | -4.25     |
| [111]      |        |           |                           |        |           |
|            | 1.425  | 0.82(5)   | $\Gamma_{30;\#}$ (sphere) | 1.193  | 0.24      |
|            | 1.600  | 1.00(4)   | $\Gamma_{30;\#}$ (sphere) | 1.328  | 0.26      |
|            | 1.740  | 3(1)      | $X_{27;\#}$ (pillow)      | 1.432  | -1.16     |
|            | 1.809  | 2(1)      | $X_{27;\#}$ (pillow)      | 1.376  | -0.64     |
|            | 1.860  | 3(2)      | $X_{27;\#}$ (pillow)      | 1.376  | -0.64     |
| 1          | 2.140  | 1.6(1)    | $X_{27;\#}$ (pillow)      | 1.833  | -0.76     |
| 2          | 2.180  |           | $X_{27;\#}$ (pillow)      |        |           |
| 1          | 2.240  | 1.9(1)    | $X_{27;\#}$ (pillow)      | 1.833  | -0.76     |
| 2          | 2.272  | 3.1(2)    | $X_{27;\#}$ (pillow)      |        |           |
| 1          | 2.307  | 1.4(3)    | $X_{27;\#}$ (pillow)      | 1.833  | -0.76     |
| 2          | 2.330  | 2.4(4)    | $X_{27;\#}$ (pillow)      |        |           |
| 1          | 3.170  | 2.20(6)   | (neck)                    |        |           |
| 2          | 3.230  | 1.60(3)   | $L_{28;\#}$ (neck)        | 3.067  | 0.53      |
| 3          | 3.260  | 1.45(5)   | (neck)                    |        |           |
|            |        |           | $L_{29;\#}$ (neck)        | 2.250  | 7.89      |
|            |        |           | $L_{28;\#}$ (neck)        | 3.517  | 1.33      |
| [001]      |        |           |                           |        |           |
|            | 0.645  | 4(2)      | $W_{27;\#}$ (pillow-neck) | 0.767  | 0.68      |
|            | 1.420  | 0.9(1)    | $\Gamma_{30;\#}$ (sphere) | 1.201  | 0.24      |
|            | 1.610  | 1.1(1)    | $\Gamma_{30;\#}$ (sphere) | 1.340  | 0.26      |
|            | 1.970  | 4(1)      | $W_{28;\#}$ (rosette)     | 2.626  | -1.28     |
|            | 2.270  | 7(2)      | $W_{28;\#}$ (rosette)     | 3.232  | -0.94     |
|            | 3.630  | 5(2)      | $W_{29;\#}$ (rosette)     | 3.699  | -7.96     |

feature of the rotation plot is the  $\Gamma_{30}$  branch which has a minimum frequency for  $\hat{B} \parallel [111]$ . Some branches, e.g.  $\Gamma_{27;\#}$  and  $\Gamma_{27;\#}$  [Fig. 1(a)], show small splittings which could arise from extremely small corrugations in the FS or a small misalignment of the sample. The  $\Gamma_{27;\#}$  branch is a signature of the neck around the L point in the [111] direction and is in excellent quantitative agreement with the neck for the minority spin ( $\downarrow$ ) of band 28. Although three sheets of the FS are predicted to have necks along the [111] directions (orbits  $L_{28;\#}$ ,  $L_{28;\#}$ ,  $L_{29;\#}$ ) only one neck-like branch is observed experimentally. The most likely reason is that the higher masses of the  $L_{28;\#}$  and  $L_{29;\#}$  orbits (see Table I) make the signals too weak to be resolved.

The topology of sheet 28 ( $\uparrow$  and  $\downarrow$  spin) is reminiscent of the FS of Cu [15]. Thus, we expect to see the other orbits seen in Cu. The  $\Gamma_{27;\#}$  and  $\Gamma_{27;\#}$  orbits near  $\hat{B} \parallel [110]$  ( $X_{28;\#}$  and  $X_{28;\#}$ ) correspond to the "dog bone" in Cu. We identify the  $\Gamma_{27;\#}$  and  $\Gamma_{27;\#}$  branches as the  $W_{28;\#}$  and  $W_{28;\#}$

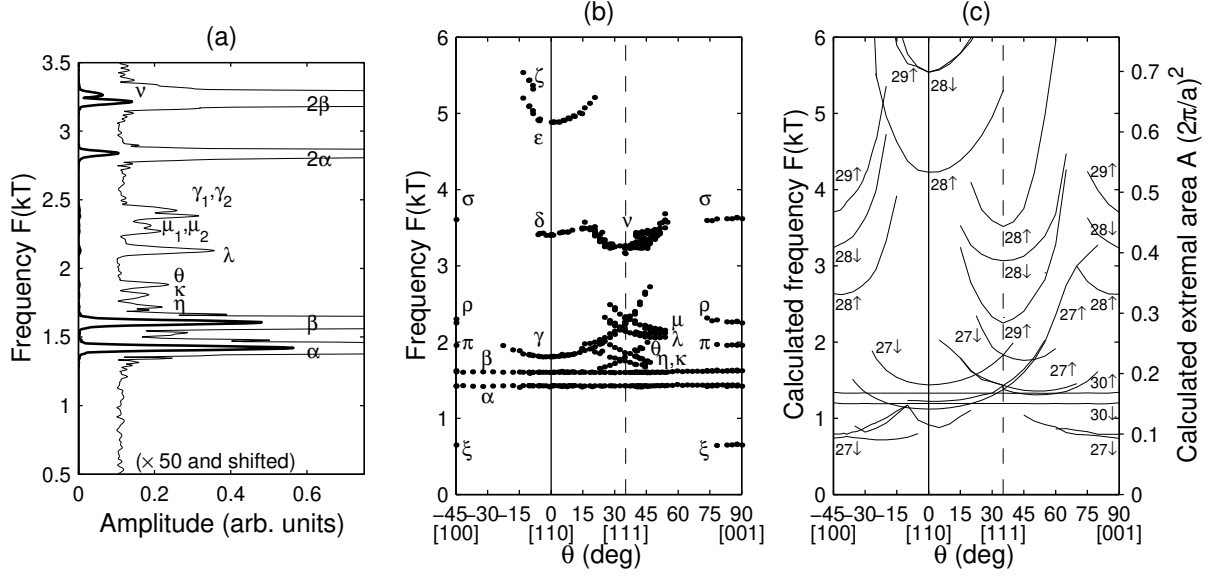


FIG. 1: (a) A dHvA spectrum collected for B applied 1.5 deg from [111] towards [001]. Data was collected in the range  $7 < B < 13.4$  T at  $T = 25$  mK. (b) The angular dependence the dHvA frequencies. (c) Calculated dHvA frequencies.

calculated orbits and as the "four-cornered rosette" orbits in Cu for fields B k [001] [15]. These orbits connect the [111] necks in neighboring Brillouin zones and are shown in Fig. 2(a). The low-frequency branch appears to be due to the  $W_{27,\#}$ . Finally, the branch appears to be due to either the rosette-type orbit  $W_{29,\#}$  of sheet 29 or an extension of the  $X_{27,\#}$  branch to [001] which may occur with a small energy shift of band 27. Our calculation overestimates the size of the "dog bone" and "rosette" orbits on sheets 28 and 29. We note that because all these orbits are related to the necks, both frequencies would be decreased if these bands were lowered relative to  $E_F$  or if the necks opened out more rapidly along [111] than the calculation predicts.

We now consider the mass enhancement of the quasiparticles in  $ZrZn_2$ . Comparison of the measured and calculated cyclotron masses shows that the mass enhancements  $m^* = m_b = 1 +$  are in the range of about 2.5 for  $B = 9.2$  T. The linear term of the specific heat shows a strong field dependence,  $C = 35 \text{ mJ mol}^{-1} \text{ K}^{-2}$  for  $B = 9.2$  T and  $47 \text{ mJ mol}^{-1} \text{ K}^{-2}$  for  $B = 0$  [16], thus we expect  $m$  to be field dependent. Comparing the measured for  $B = 9.2$  T with  $m_{\text{calc}} = (2/3)k_B^2 N_{\text{tot}}(E_F) = 9.6 \text{ mJ mol}^{-1} \text{ K}^{-2}$  [17] we find an average mass enhancement  $m^* = m_b = 3.7$  which is in the center of the range observed by dHvA. If we make the same calculation for  $B = 0$ , we find  $m^* = m_b = 4.9$ . To our knowledge, no other alloy of 3d-band metals shows mass enhancements close to these. Palladium which is often taken as an example of a system with strong spin fluctuations has an enhancement of about two.

Table II summarizes the important parameters for

TABLE II: Selected measured (calculated) Fermi surface parameters for  $ZrZn_2$  [20].

| branch (orbit)                   | (30;#)      | (30;")      | (X <sub>27</sub> ;#) | (K <sub>28</sub> ;") |
|----------------------------------|-------------|-------------|----------------------|----------------------|
| $F$ (kT)                         | 1.42 (1.19) | 1.60 (1.33) | 1.81 (1.38)          | 4.77 (5.54)          |
| $h k_F / \pi$ (Å <sup>-1</sup> ) | 0.21 (0.19) | 0.22 (0.20) | 0.23 (0.20)          | 0.38 (0.41)          |
| $m^* / m_b$ ( $m_e$ )            | 0.82 (0.24) | 0.95 (0.26) | 1.27 (-0.51)         | 3.9 (-1.53)          |
| $v_F$ (M m s <sup>-1</sup> )     | 0.30 (0.92) | 0.27 (0.90) | 0.21 (0.45)          | 0.11 (0.31)          |
| (ps)                             | 0.28        | 0.31        | 0.32                 |                      |
| $l$ (Å)                          | 2580        | 2750        | 1500                 |                      |

some FS orbits in  $ZrZn_2$ . The measured Fermi velocity and cyclotron mass include the effects of electron correlations. The quasiparticle lifetime and mean-free-path,  $l$ , are determined from the Dingle factor  $R_D$ . It is interesting to note that  $l \approx 1500$  (2800 Å) is considerably larger than the superconducting coherence length  $\xi \approx 270$  Å in this superconducting sample allowing the possibility of unconventional superconductive pairing [6].

It is interesting to compare the properties of  $ZrZn_2$  with other d-band ferromagnets. Fig. 2(b) shows the paramagnetic DOS for  $ZrZn_2$ . The Fermi level,  $E_F$ , lies in a region where the DOS is large due to the 4d Zr band. Also shown on Fig. 2(b) are the relative shifts of  $E_F$  for both spins in the ferromagnetic state. The small exchange splitting ( $\approx 70$  meV) of  $ZrZn_2$  means that the Fermi levels for both spins remain in the high DOS region giving  $ZrZn_2$  its unusually large DOS in the ferromagnetic state in contrast with Fe and Ni (Table III). In the "stronger" ferromagnets,  $N_{\text{tot}}(E_F)$  is considerably

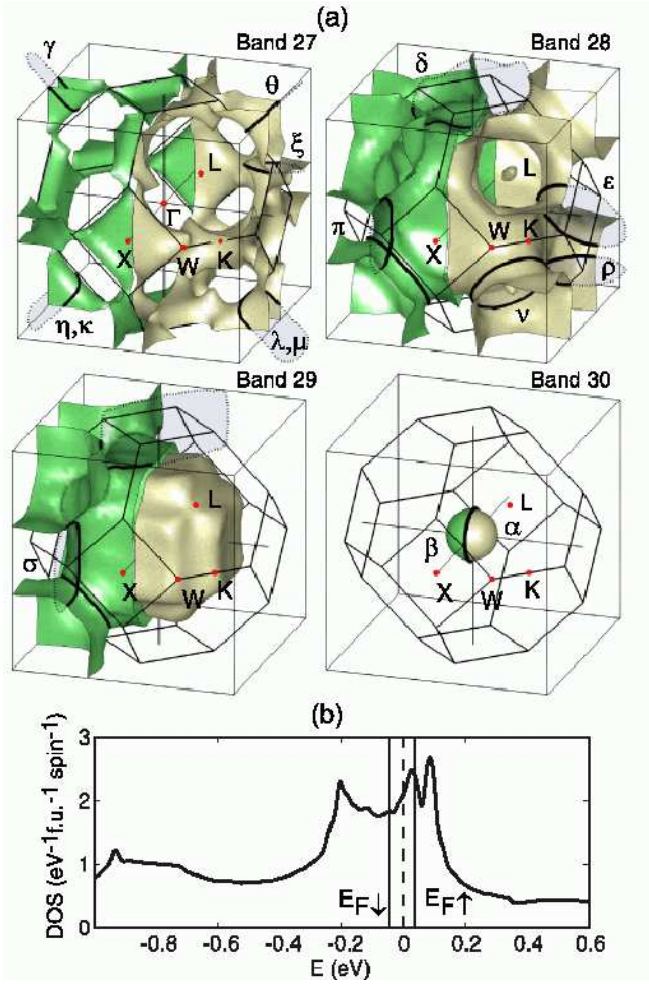


FIG. 2: (a) Calculated Fermi surface of  $\text{ZrZn}_2$  for the four bands crossing the Fermi level. The left and right parts of each figure are the majority (") and minority (#) spin sheet respectively. The labeled solid lines are some of the orbits discussed in the text. (b) The calculated DOS for paramagnetic  $\text{ZrZn}_2$  (see text). The vertical solid lines represent the energy shift of the spin- and # Fermi energies in the ferromagnetic state.

TABLE III: Comparison of band parameters (magnetic moment,  $\mu_B$ , exchange splitting,  $\Delta$ , DOS at  $E_F$  between  $\text{ZrZn}_2$  and some d-band ferromagnets [18]

|  | Fe   | Ni   | $\text{ZrZn}_2$ |
|--|------|------|-----------------|
| $n_{\text{e}} = n_{\text{+}} - n_{\text{-}} \text{ (} \mu_B \text{ / f.u.)}$ | 2.12 | 0.56 | 0.16            |
| $\Delta \text{ (eV)}$  | 2.2  | 0.6  | 0.07            |
| $N_{\text{+}}(E_F) \text{ (eV}^{-1} \text{f.u.}^{-1} \text{spin}^{-1})$      | 0.83 | 0.17 | 2.39            |
| $N_{\text{-}}(E_F) \text{ (eV}^{-1} \text{f.u.}^{-1} \text{spin}^{-1})$      | 0.25 | 1.50 | 1.80            |
| $N_{\text{tot}}(E_F) \text{ (eV}^{-1} \text{f.u.}^{-1})$                     | 1.08 | 1.67 | 4.19            |

less in part due to the larger exchange splitting moving  $E_F$  for one of the spin out of the d-band. A high density DOS at the Fermi energy generally favors superconductivity so this may be a key factor in understanding the superconductivity in this material.

In summary, we have used angle-resolved dHvA measurements to characterize the Fermi surface of the ferromagnetic superconductor  $\text{ZrZn}_2$ . Our observations are in good agreement with an ab-initio LSDA band structure calculation and shed light on some of the unique properties of  $\text{ZrZn}_2$ . We find that  $\text{ZrZn}_2$  has a very large DOS at  $E_F$  compared to other d-band ferromagnets both because of the presence of several large sheets of FS and because the Fermi levels for both majority and minority spins lie in the Zr d-band in the ferromagnetic state. Further, the fermion quasiparticles are strongly enhanced with an average mass enhancement of about 4.9. This value is large for materials containing only d-band metallic elements and comparable with that found in the oxide system  $\text{Sr}_2\text{RuO}_4$  [19]. The presence of the high density of quasiparticles naturally explain the very large electronic heat capacity observed in  $\text{ZrZn}_2$  and also explains the unsaturated magnetic moment (or large intrinsic magnetic susceptibility) in the ferromagnetic state. Finally, the high quasiparticle DOS will favor superconductivity.

We are grateful to N.R. Bernhoeft, B.L. Gyorffy, G.G. Lonzarich, Zs. Major, C.P. Eiderer and J.B. Staunton for their help with this work. Support from the EP-SRC, the Swiss National Science Foundation (GS) and the Royal Society (PJM and SBD) is also acknowledged.

- 
- [1] S.S. Saxena et al, Nature (London) 406, 587 (2000).
  - [2] C.P. Eiderer et al, Nature (London) 412, 58 (2001).
  - [3] D. Aoki et al, Nature (London) 413, 613 (2001).
  - [4] K. Shimizu et al, Nature (London) 412, 316 (2001).
  - [5] N.E. Berk and J.R. Schrieffer, Phys. Rev. Lett. 17, 433 (1966); D. Fay and J. Appel, ibid 22, 3173 (1980).
  - [6] A.P. Mackenzie et al, Phys. Rev. Lett. 80, 161 (1998).
  - [7] K. Ishida et al, Nature (London) 396, 658 (1998).
  - [8] D.J. Singh and I.I. Mazin, Phys. Rev. Lett. 88, 187004 (2002).
  - [9] P.C. Canfield, P.L. Gammel and D.J. Bishop, Physics Today 51, 40 (1998); I. Felner et al, Phys. Rev. B 55, R3374 (1997).
  - [10] D. Shoenberg, Magnetic Oscillations in Metals (Cambridge, 1984).
  - [11] L.W. M. Schreurs et al, Mat. Res. Bull. 24, 1141-5 (1989).
  - [12] P.G. M. Attkins and A.E. Dixon, J. Phys. F 11, L147 (1981); J.M. van Ruitenbeck et al, J. Phys. F 12, 2919 (1982); A.P.J. van Deursen et al, J. Mag. Mag. Mat. 54-57, 1113 (1986); I. Lo and S. Mazumdar and P.G. M. Attkins, Phys. Rev. Lett. 62, 2555 (1989).
  - [13] G. Santi, S.B. Dugdale and T. Jarlborg, Phys. Rev. Lett. 87, 247004 (2001).
  - [14] R.A. de Groot, D.D. Koelling, and F.M. Mueller, J. Phys. F 10, L235 (1980); T. Jarlborg, A.J. Freeman and D.D.

- Koelling, J. *Magn. Magn. Mater.* 23-291 (1981).
- [15] A. B. Pippard, *Phil. Trans. Roy. Soc. A* 250, 325 (1957); D. Schoenberg, *ibid A* 255, 85 (1962); A. S. Joseph et al., *Phys. Rev.* 148, 569 (1966). See also Ref. 10.
- [16] C. Pfeiderer et al., *J. Magn. Magn. Mater.* 226-260, 258 (2001).
- [17] We neglect the field dependence of  $N_{\text{tot}}(E_F)$ , which we estimate to be about 10% for  $B = 10$  T.
- [18] J. Callaway and C. S. Wang, *Phys. Rev. B* 16, 2095 (1977); C. S. Wang and J. Callaway, *ibid* 15, 298 (1977).
- [19] A. P. Mackenzie et al., *Phys. Rev. Lett.* 76, 3786 (1996).
- [20] We calculate the FS parameters as follows:  $\hbar k_F = \sqrt{2m_F E_F}$ ,  $A = \frac{1}{2} v_F = \frac{\hbar k_F}{m_F}$ ,  $l = v_F = \frac{\hbar k_F}{m_F}$ .